Spin polarization of the two-dimensional electron gas at the EuO/$SrTiO_3$ (001) interface

Paul Rosenberger,[1,2] Andri Darmawan,[3] Olena Fedchenko,[2] Olena Tkach,[2] Serhii V. Chernov,[4] Dmytro Kutnyakhov,[5] Moritz Hoesch,[5] Markus Scholz,[5] Kai Rossnagel,[6,7] Rossitza Pentcheva,[3] Gerd Schönhense,[2] Hans-Joachim Elmers,[2] and Martina Müller[1,*]

[1]*Fachbereich Physik, Universität Konstanz, 78457 Konstanz, Germany*
[2]*Institut für Physik, Johannes Gutenberg-Universität, 55099 Mainz, Germany*
[3]*Department of Physics and Center for Nanointegration (CENIDE), Universität Duisburg-Essen, Lotharstr. 1, 47057 Duisburg, Germany*
[4]*Department of Physics and Astronomy, Stony Brook University, Stony Brook, New York 11794, USA*
[5]*Deutsches Elektronen-Synchrotron DESY, 22607 Hamburg, Germany*
[6]*Institut für Experimentelle und Angewandte Physik, Christian-Albrechts-Universität zu Kiel, 24098 Kiel, Germany*
[7]*Ruprecht Haensel Laboratory, Deutsches Elektronen-Synchrotron DESY, 22607 Hamburg, Germany*

(Received 8 January 2025; accepted 23 April 2025; published 2 June 2025)

Spin-polarized two-dimensional electron gases (2DEGs) are of particular interest for functional oxide electronics applications. The redox-created 2DEG residing on the strontium titanate, $SrTiO_3$ (STO), side of a europium monoxide (EuO)/$SrTiO_3$ (001) interface is expected to be significantly spin polarized due to the proximity to the strong ($7\,\mu_B/f.u.$) Heisenberg ferromagnet EuO. We apply magnetic circular dichroism in the angular distribution (MCDAD) of photoemitted electrons to investigate whether and how the induced spin polarization of the 2DEG depends on the dimensionality of the overlaying EuO layer. The experimental data are complemented by density functional theory calculations with a Hubbard U term (DFT + U). We show that the EuO/STO interfacial 2DEG is spin polarized even for ultrathin EuO overlayers, starting at an EuO threshold thickness of only two monolayers. Additional EuO monolayers even increase the induced magnetic Ti moment and thus the spin polarization of the 2DEG. Our results and the potential to enhance the magnetic order of EuO by other proximity effects indicate that the EuO/STO(001) interface is an ideal template for creating (multi-)functional spin-polarized 2DEGs for application in oxide electronics.

DOI: 10.1103/PhysRevMaterials.9.064401

I. INTRODUCTION

The observation of a conducting interface between the large band gap insulators $LaAlO_3$ and $SrTiO_3$ [1] sparked the scientific interest in oxide heterostructures with emergent properties. The two-dimensional electron gas (2DEG) near the interface can exhibit paramagnetism and ferromagnetism and even coexist with superconductivity [2,3]. The origin of the 2DEG [4] is either associated with a charge transfer at the interface to avoid diverging electric fields at the interface [5,6], or with oxygen vacancies at the $SrTiO_3$ surface that arise during growth [7,8]. The oxygen vacancies are present in crystalline oxide films that are grown under reducing environments [9,10]. Oxygen vacancies in $SrTiO_3$ act as donors [11] and contribute charge carriers to the 2DEG. The corresponding states in the band gap were observed by angle-resolved photoemission spectroscopy [12,13]. For functional oxide (spin-)electronic devices, it would be highly interesting to form a spin-polarized 2DEG at the interface. Spin-polarized 2DEGs at the interfaces of oxides have been observed for $LaAlO_3/BaTiO_3$ [14], $SrMnO_3/LaMnO_3$ [15], and heterostructures with $EuTiO_3$ [16–20], as well as for EuO/$KTaO_3$ [21].

EuO/$SrTiO_3$ interfaces have attracted large interest [12,22–26] because the conductivity mismatch in metal/semiconductor junctions can be overcome by the ferromagnetic (FM) semiconductor EuO [27–29]. Therefore, the EuO/$SrTiO_3$ system could be used to fabricate a spin-metal-oxide-semiconductor field-effect transistor [30]. Recent studies show that the magnetic order of EuO can be enhanced and also designed by magnetic proximity coupling to magnetic transition metals of the 3*d* group [31,32]. This overcomes the relatively low Curie temperature of EuO (69 K) in the coupled 3*d* FM/EuO bilayer, which behaves like a strong synthetic ferrimagnet. Furthermore, EuO exhibits a large (0.6 eV) exchange splitting in the conduction band [33–36]. If the vacancy-induced carriers are located at the EuO side of the interface, it could result in a 100% spin-polarized 2DEG [37]. However, previous experiments show that due to the band alignment at the interface, the vacancy-induced carriers reside mostly within $SrTiO_3$ [12,22]. Thus, it is not yet clear whether the interface states formed at the EuO/$SrTiO_3$ interface are spin polarized or not. In this article, we show that the interface states are indeed spin polarized. We apply circular dichroism in the angular distribution of direct photoemitted electrons to demonstrate a spontaneous breaking of the time-reversal symmetry of the interface states, which is a clear signature

*Contact author: martina.mueller@uni-konstanz.de

of finite spin polarization of these states. Further insights on the electronic reconstruction and spin polarization of few monolayers (ML) EuO on $SrTiO_3$ (001) are obtained from density functional theory calculations with a Hubbard U term (DFT + U).

II. EXPERIMENTAL DETAILS

A. Sample preparation and handling

We have prepared EuO ultrathin films on TiO_2-terminated $SrTiO_3$:Nb substrates (Crystec GmbH) using molecular beam epitaxy (MBE) in ultrahigh vacuum (UHV). The base pressure of the oxide MBE system at University of Konstanz was $p_{MBE} \leqslant 2 \times 10^{-10}$ mbar. Prior to EuO growth, the substrates were annealed in UHV for 30 min at $T_S = 500\,^{\circ}$C. EuO films of thicknesses of one, two, and four monolayers were redox grown as described elsewhere [26]. The substrate was kept at room temperature during deposition. Eu metal was evaporated from a Knudsen cell at a rate of $r_{Eu} = 0.005$ Å/s. The rate was measured with a quartz crystal microbalance. Subsequent *in situ* x-ray photoelectron spectroscopy (XPS) was applied to confirm the stoichiometry of the deposited EuO film as well as the partial reduction of Ti^{4+} in the substrate to Ti^{3+}, indicative for the formation of the interfacial two-dimensional electron gas [26]. An ultrahigh vacuum suitcase was used to transfer the samples *in vacuo* to the beam line P04 at PETRA III (DESY, Hamburg) [38].

After transferring a sample to the liquid helium (LHe) cooled sample stage it was magnetized by approaching a permanent magnet. The measurement was then performed with the sample in the remanent magnetic state.

B. Setup

For the photoemission measurements at beam line P04 (PETRA III, DESY Hamburg), photoelectrons were excited by circularly polarized soft x-rays. We used a time-of-flight momentum microscope (MM) at the open port I of P04 with an energy resolution of 60 meV at a sample temperature of 30 K [39–41]. The photoemission experiments were performed with an incidence angle of the photon beam of 22° with respect to the sample surface, and the azimuthal orientation of the sample has been adjusted so that the photon incidence plane coincides with the (100) axis of the $SrTiO_3$ substrate. The coordinate system for the photoelectron momentum (k_x, k_y, k_z) was set to k_z along the crystallographic [001] direction, i.e., surface normal, k_x along [100] and k_y along [010] in-plane directions, respectively.

III. RESULTS

A. *In situ* sample characterization

For all three samples, XPS of the Ti 2p core level revealed the formation of Ti^{3+} upon Eu metal deposition, indicating redox-driven formation of a 2DEG at the metal oxide/STO interfaces [26]. From XPS of the Eu $3d_{5/2}$ core level we find that EuO is formed with contributions of metallic Eu. The proportion of metallic Eu increases with increasing EuO thickness. This trend was expected because the oxygen ion conductivity of a material not only increases with increasing temperature but is also an important driving parameter for the interfacial redox reaction [26,42–44]. We consider the off stoichiometry an advantage. Eu(O) oxidizes even when stored under UHV conditions [45]. Hence, a sample that is perfectly stoichiometric immediately after preparation in the laboratory will contain some undesired Eu^{3+} when investigated later at the synchrotron. In contrast, in a sample that initially contains Eu metal, Eu^0, will oxidize to Eu^{2+}, i.e., EuO, before the sample starts to degrade by overoxidation. Therefore, our samples do not degrade but ripen in the storage time between preparation in the laboratory and measurement at P04. LEED and RHEED suggest the absence of long-range order of the redox-grown EuO films.

B. Momentum microscopy

To investigate the proximity-induced magnetic order of the 2DEG at the EuO/STO interface and its dependence on the EuO thickness, we performed ToF-MM measurements of the valence band using left and right circularly polarized light (intensities I^- and I^+, respectively). The photon energy was set to $h\nu = 466$ eV, i.e., to the Ti L_2 resonance, to enhance the signal from the buried interface [46].

Figures 1(i), 1(ii), and 2 show maps of the photoemission intensities and asymmetries of the samples with EuO thicknesses of 2 ML, 4 ML, and 1 ML, respectively. In each figure, from left to right these are the sum intensity as a function of binding energy E_B and parallel momentum k_x and k_y,

$$I_{sum}(E_B, k_x, k_y) = I^+(E_B, k_x, k_y) + I^-(E_B, k_x, k_y)\,, \qquad (1)$$

the asymmetry,

$$A(E_B, k_x, k_y) = \frac{I^+(E_B, k_x, k_y) - I^-(E_B, k_x, k_y)}{I_{sum}(E_B, k_x, k_y)}\,, \qquad (2)$$

the circular dichroism in the angular distribution (CDAD) [47],

$$\mathrm{CDAD}(E_B, k_x, k_y) = [A(E_B, k_x, k_y) - A(E_B, k_x, -k_y)]/2\,, \qquad (3)$$

and the magnetic circular dichroism in the angular distribution (MCDAD) [48,49],

$$\mathrm{MCDAD}(E_B, k_x, k_y) = [A(E_B, k_x, k_y) + A(E_B, k_x, -k_y)]/2\,. \qquad (4)$$

In Figs. 1 and 2 the asymmetry, CDAD and MCDAD are shown in a two-dimensional color scale. This results in a contrast (blue to red) only being displayed if the corresponding intensity is significant.

The following maps of the four measures are shown: top: $N(E_B = 50\,\mathrm{meV}, k_x, k_y)$; middle: $N(E_B, k_x, k_y = 0)$; bottom: $N(E_B, k_x = 0, k_y)$, where N denotes I, A, CDAD, and MCDAD, respectively. Note that by definition the CDAD at $k_y = 0$ vanishes. Therefore, in Fig. 2(g), we present the section $k_y \approx 0.02$ Å^{-1}. The data were twofold symmetrized, i.e., in our representations it is $N(k_x) = N(-k_x)$.

We first discuss the results for the ferromagnetic 2 ML and 4 ML EuO on STO:Nb sample. For the samples with 2 ML and 4 ML EuO on STO:Nb, a blurred yet well-resolved (band) structure can be observed in the sum intensity images, Figs. 1 and 2, panels (a), (e), (i). Figures 1 and 2, panel (a), show the

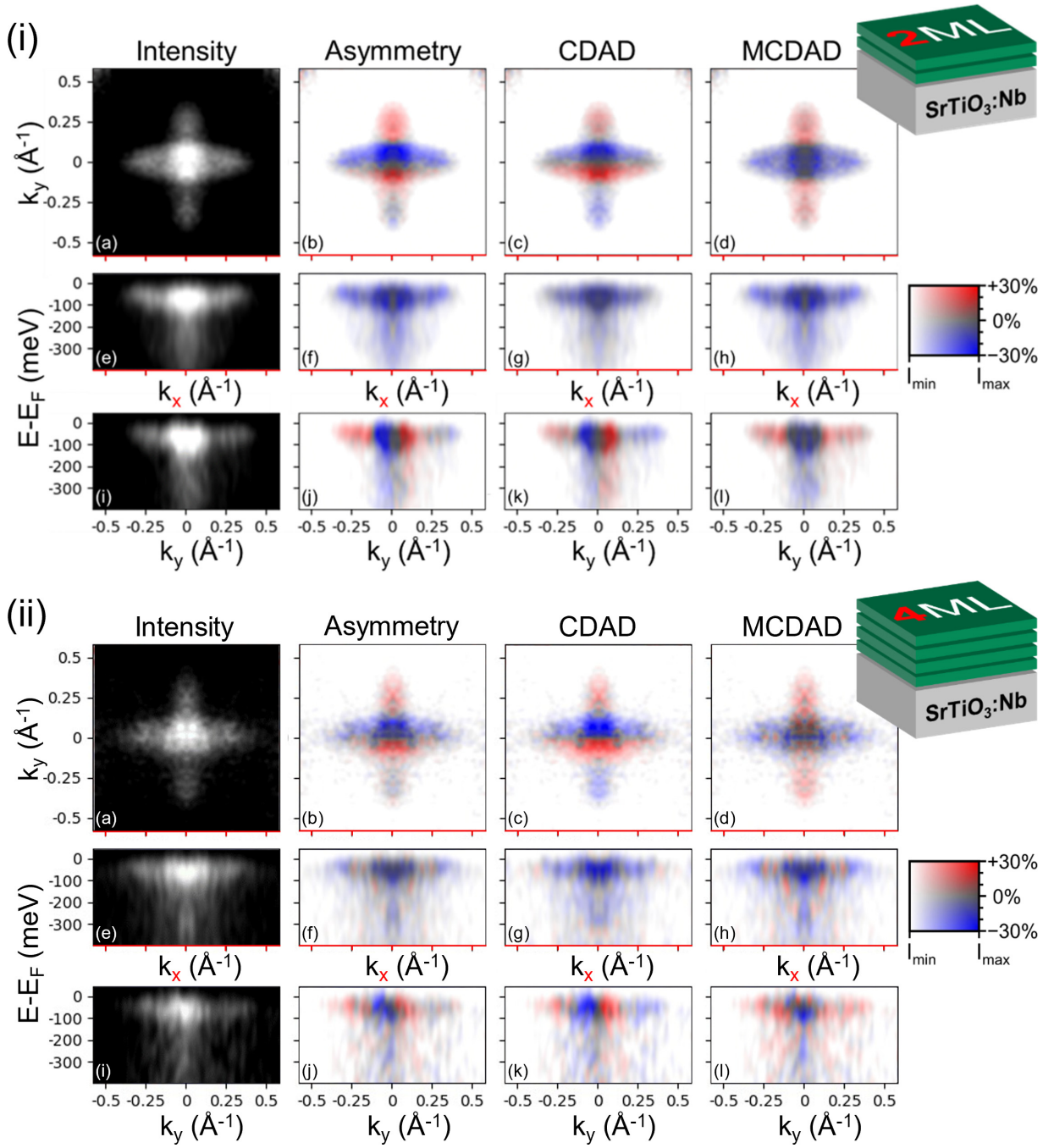

FIG. 1. Photoemission maps obtained from the samples with (i) two, and (ii) four monolayers EuO on STO:Nb. Intensity, asymmetry, CDAD and MCDAD are shown (from left to right), each as functions of k_x and k_y at $E_B = 50$ meV (top), k_x and E_B at $k_y = 0$ (middle; for CDAD: $k_y \approx 0.02$ Å^{-1}), as well as k_y and E_B at $k_x = 0$ (bottom). All maps exhibit strong features: The intensity maps reveal the presence of the interfacial 2DEG. The asymmetry is pronounced and yields both a strong CDAD and MCDAD. The CDAD suggests that the bands extending along k_x and k_y are of different orbital character. The nonvanishing MCDAD indicates a finite spin polarization of the 2DEG.

Fermi surfaces around the Γ point. Figures 1 and 2, panels (e) and (i), are the corresponding energy-momentum maps revealing the electronic band structure along k_x and k_y, respectively. They reveal parabolic structures extending from E_F to the band bottoms at approximately -150 meV and -400 meV, respectively. The corresponding widths of the structures along k are $\approx$0.75 Å^{-1} and $\approx$0.3 Å^{-1}. These widths match well with those estimated from an earlier angle-resolved photoelectron spectroscopy (ARPES) study of the EuO/STO 2DEG for the Ti $3d_{xz/yz}$ and Ti $3d_{xy}$ sub-bands [26]. We therefore state that our sum intensity images, Figs. 1(i) and 1(ii), panels (a), (e), (i), confirm that the interfacial 2DEG was formed.

For both samples, a strong asymmetry A is observed [Figs. 1(i) and 1(ii), panels (b), (f), (j)] showing a similar pattern. The asymmetry is larger for the 2 ML sample compared to the 4 ML sample. This can be explained by the limited

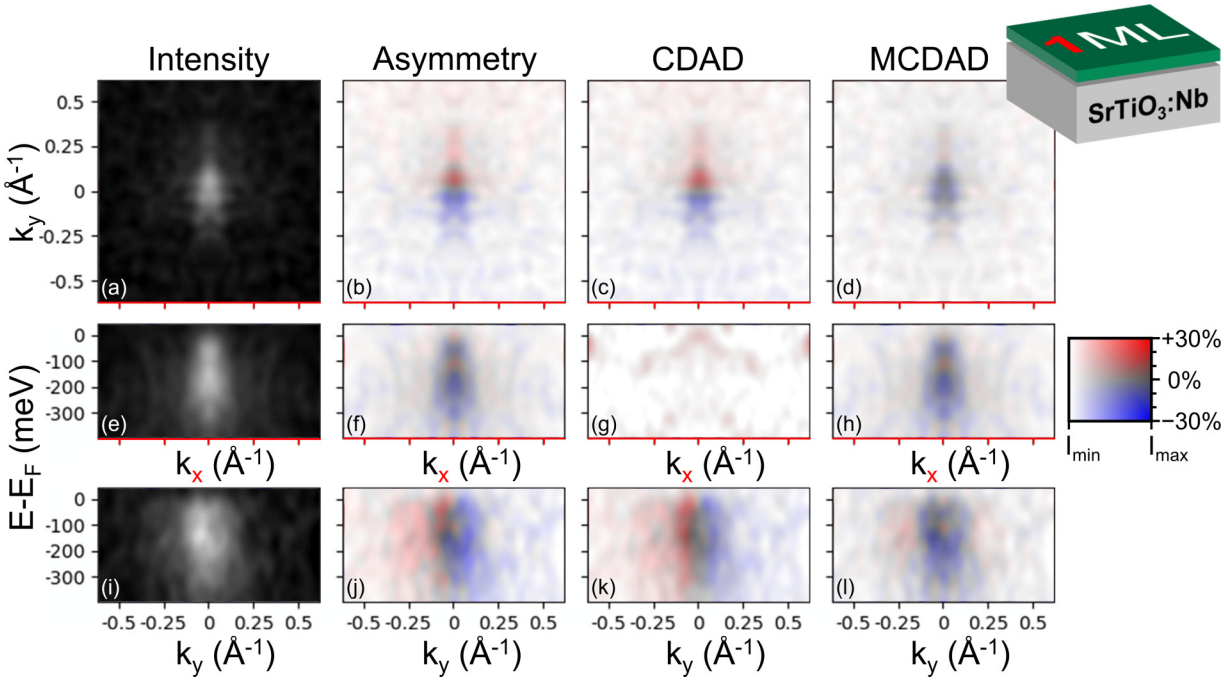

FIG. 2. Photoemission maps obtained from the sample with one monolayer EuO on STO:Nb. Intensity, asymmetry, CDAD, and MCDAD are shown (from left to right), each as functions of k_x and k_y at $E_B = 50$ meV (top), k_x and E_B at $k_y = 0$ (middle; for CDAD: $k_y \approx 0.02$ Å^{-1}), as well as k_y and E_B at $k_x = 0$ (bottom). The weak features in the intensity maps suggest that the redox-formed interfacial 2DEG is only weak. Asymmetry and CDAD have positive values for $k_y > 0$ and negative values for $k_y < 0$. The features do not resemble those of the other samples. The MCDAD pattern does also not match those of the other samples and the contrast (blue to red) is only small. This reflects either the limited SNR or a different electronic structure than that of the other samples.

inelastic mean free path of the photoexcited electrons. The thicker EuO layer scatters photoexcited electrons, destroying the momentum information they carry.

The CDAD calculated from A [Figs. 1(i) and 1(ii), panels (c), (g), (k)] is essentially antisymmetric with respect to the k_x axis as forced by definition. Small deviations from the antisymmetry in our representation result from the nonsymmetrized sum intensity. The band extending along the k_x-axis close to $k_y = 0$ has the opposite sign compared to the band along the k_y axis, indicating a different orbital character of these two bands. Similar patterns appear for both the 2 ML and the 4 ML sample.

The MCDAD shown in Figs. 1(i) and 1(ii), panels (d), (h), (i), reveals nonzero values in the region of the interface bands with a similar pattern for the 2 ML and 4 ML sample. The non-vanishing MCDAD indicates a time-reversal symmetry breaking that can only be explained by a nonvanishing spin polarization of the interface bands. The sign of the MCDAD does not necessarily reflect the sign of the spin polarization, as it results from a combination of exchange splitting and spin-orbit interaction [49].

For a quantitative comparison, the momentum distribution curves (MDCs) along the k_x and k_y axes are shown in Fig. 4. To increase the signal-to-noise ratio (SNR) the MDCs are averaged by ± 0.06 Å^{-1} along the perpendicular momentum axis. The maximum MCDAD signal amounts to $\pm 0.3\, I_{max}$ for the 2 ML sample and $\pm 0.2\, I_{max}$ for the 4 ML sample.

The single monolayer of EuO on STO:Nb shows a different behavior. The photoemission intensity is comparatively low [Figs. 2(a), 2(e), and 2(i)] and does not show the cross-shaped pattern observed for the 2 ML and 4 ML sample. Thus, the 2DEG at the EuO/STO interface is weak. The asymmetry A shown in Fig. 2(b) has positive values for $k_y > 0$ and negative values for $k_y < 0$. The corresponding CDAD [Figs. 2(b), 2(f), and 2(j)] clearly shows plus/minus features but appears distinct from the CDAD observed for the 2 ML and 4 ML samples. It is positive for $k_y > 0$ and negative for $k_y < 0$.

The MCDAD [Figs. 2(b), 2(f), and 2(j)] shows only small positive or negative values and does not resemble the cross-shaped pattern observed for the 2 ML and 4 ML sample. The bare MCDAD, i.e., without normalization to the sum intensity, shown in Fig. 3 proves that the absence of the MCDAD feature is real and not an artifact of the normalization. Hence, the observed MCDAD of the single monolayer

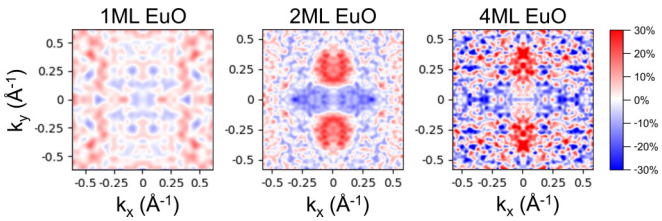

FIG. 3. MCDAD for the three samples at $E_B = 50$ meV (see right color scale for the MCDAD values). While the MCDAD features of the 2 ML (middle) and the 4 ML (right) samples are similar and resemble the shape in the representation shown in Fig. 1, the MCDAD of the single monolayer sample (left) shows an irregular pattern.

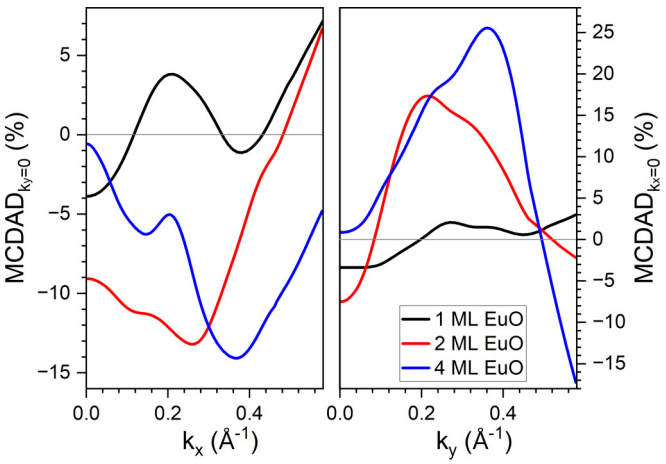

FIG. 4. MDCs along k_x (left) and k_y (right) of the three samples displaying the averaged MCDAD of -0.06 Å$^{-1} < k_y < +0.06$ Å^{-1} and -0.06 Å$^{-1} < k_x < +0.06$ Å^{-1}, respectively, at $E_B = 50$ meV. The data are smoothed by locally weighted scatterplot smoothing over a span of ≈0.24 Å^{-1}.

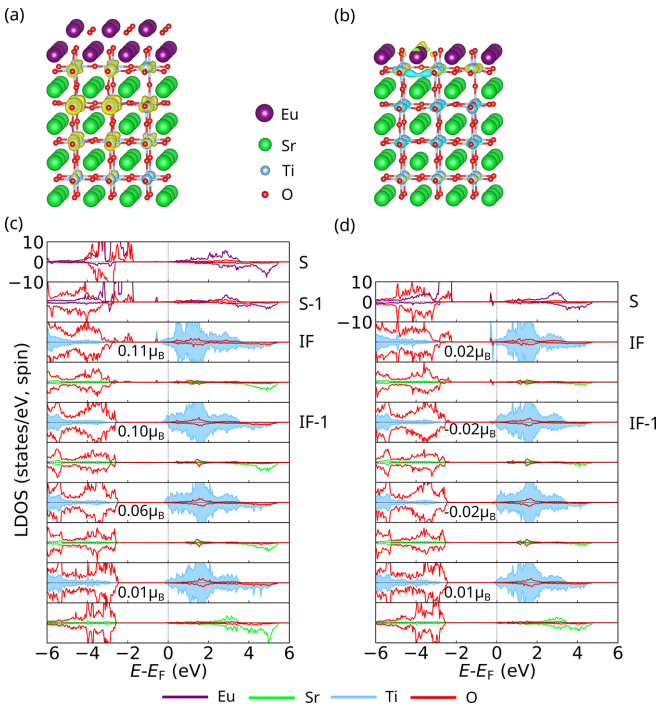

FIG. 5. Side view of the relaxed structure and spin density of (a) 2 ML EuO and (b) 1 ML EuO on STO(001) with an oxygen vacancy in the topmost TiO_2 layer and the second vacancy in the subsurface SrO layer. The spin density of 1–2 ML EuO on STO(001) is integrated between -0.4 eV and the Fermi level. Yellow and cyan areas indicate positive and negative spin density, respectively. Layer-, element-, and spin-resolved density of states of (c) 2 ML EuO on STO(001) and (d) 1 ML EuO on STO(001) together with the average of Ti magnetic moment for each TiO_2 layer in μ_B.

sample might be explained by the limited SNR or it reflects a different electronic structure. Only the dispersion curve along the k_y axis shown in Fig. 2(l) exhibits a pattern similar to that of the 2 and 4 ML samples. In contrast, the MDC shown in Fig. 4 is sizable with respect to that of the other samples only along the k_x axis. However, it not only differs from the MDCs of 2 ML and 4 ML but its amplitude is comparable to that of the negligible MDC along k_y. This supports our assumption that the features obtained for a single monolayer are due to an insufficient SNR or of different physical origin than those observed for 2 ML and 4 ML EuO/STO.

IV. THEORETICAL MODELING

To shed more light on the electronic reconstruction at the $EuO/SrTiO_3$ (001) interface we performed DFT + U calculations using the Vienna *ab initio* simulation package (vasp) [50,51] with the projector augmented wave (PAW) [52,53] basis and the PBEsol approximation for the exchange correlation functional [54]. The DFT + U approach within the Dudarev's scheme [55] was used with an on-site Hubbard U term of 2 eV and 7.5 eV for the Ti $3d$ and Eu $4f$ states, respectively. The latter value leads to a very good agreement with angle-integrated valence band spectra [20] concerning the position of the localized Eu $4f$ states. The system consists of 1 or 2 ML of EuO (rotated by 45°) on top of STO(001) where the Eu ion is located at a tentative Sr site on top of the TiO_2 layer that was reported previously to be the most stable configuration [12,22]. We employed a $2a \times 3a \times 4a$ STO(001) slab with two oxygen vacancies including 20 Å vacuum region to prevent any interaction between the slab and its periodic images. The first oxygen vacancy is located in the topmost TiO_2 layer and the second is in the SrO subsurface layer with a distance of 6.2 Å [Figs. 5(a) and 5(b)]. This configuration was found previously to be most suitable to model the 2DEG at the STO(001) [56] and ETO(001) [20]. The lateral lattice constant is fixed to the experimental value of STO, 3.905 Å, while the calculated bulk EuO lattice constant is 5.18 Å. Thus the EuO layer is subject to 6.6% tensile strain. We used a plane-wave cutoff energy of 400 eV and sampled the Brillouin zone with $6 \times 4 \times 1$ Monkhorst-pack k points. The ionic positions are fully relaxed until the forces were less than 0.01 eV/Å.

A side view of the relaxed structure and spin density and the layer-resolved density of states (LDOS) of 2 and 1 ML of EuO on STO(001) is shown in Fig. 5. Both the spin density and LDOS indicate the formation of a spin-polarized 2DEG in particular for the 2 ML EuO on STO(001): the averaged Ti magnetic moment in the topmost TiO_2 layer is ∼0.11 μ_B/Ti for 2 ML EuO on STO(001) and 0.02 μ_B/Ti for 1 ML EuO on STO(001). For 3 ML EuO (not shown), the Ti magnetic moment is even larger than for 2 ML, i.e., ∼0.16 μ_B/Ti. While the localized Eu $4f$ states lie below -2 eV, localized in-gap Ti $3d$ state appears at -0.5 eV in the majority spin channel, which hybridizes with Eu $5d$ states. The in-gap state is aligned ferromagnetically with the Eu $4f$ spins due to the proximity effect. Furthermore, dispersive spin-polarized contributions to the 2DEG between -0.3 eV and E_F are observed both in the interface and the neighboring deeper layer. In contrast, the spin polarization is nearly quenched in the case of 1 ML EuO on STO(001), the localized in-gap states lying closer to the Fermi level appear in both spin channels, thus their contributions cancel out.

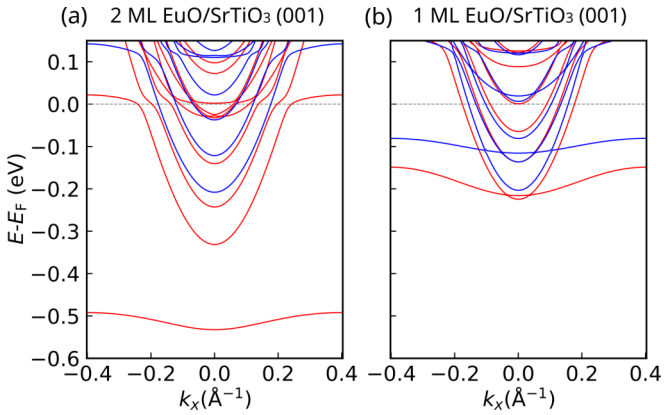

FIG. 6. DFT + U spin-resolved electronic band structure of (a) 2 ML EuO on STO(001) and (b) 1 ML EuO on STO(001) along $\Gamma - X$ direction. Red/blue denotes majority/minority bands.

The spin-resolved band structure of 2 and 1 ML EuO on STO(001) presented in Figs. 6(a) and 6(b) shows significant differences in the two cases. The dispersive majority bands of d_{xy} character reach much deeper below the Fermi level (up to -0.35 eV) for 2 ML EuO on STO(001) than for 1 ML EuO on STO(001) (-0.23 eV). Moreover, the exchange splitting is one order of magnitude larger in the former case. In the latter case the localized band in the majority channel lies 0.1 eV lower than in the minority channel. Overall, the band structure confirms the much more robust spin polarization for 2 ML than for 1 ML EuO on STO(001), consistent with experiment.

Figure 7 shows the direct comparison of experimental and theoretical data for the 2 ML case. We find that the parabolic behavior of the shallow and steep bands are well captured. However, the corresponding binding energies of theory and experiment deviate, which we attribute to the insufficient consideration of electron correlation effects.

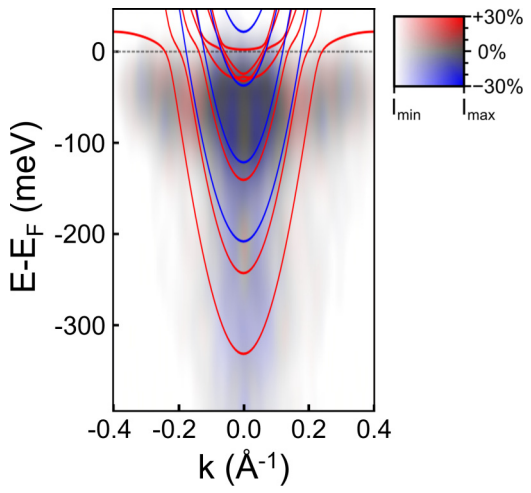

FIG. 7. Joint representation of experimental MCDAD and calculated spin-polarized band structure for 2 ML EuO/STO. Since DFT + U does not consider anisotropy and therefore is equivalent along k_x and k_y, the experimental data along k_x and k_y of sum intensity and MCDAD, respectively, were averaged. An offset was accounted for by adding a constant value to the MCDAD (≈10% of its range), i.e., by slightly shifting colors from blue to red.

V. DISCUSSION

Our present study addresses the spin polarization of the redox-created 2DEG at the EuO/STO(001) interface by means of circular dichroism in ToF-MM and DFT + U calculations. Both experiment and theory reveal that an EuO film as thin as 2 ML induces a magnetic moment in the thus spin-polarized 2DEG residing at the STO side of the interface. The induced magnetic moment is ferromagnetically aligned with the magnetization of the EuO overlayer. In contrast, no sizable MCDAD signal is observed for a single EuO ML, indicating that spin polarization is absent. This is in line with the DFT + U calculations, suggesting that the induced Ti magnetic moment for a system with a single EuO monolayer is less than 20% of the magnetic moment induced by 2 ML EuO. This is supported by previous SQUID (superconducting quantum interference device) magnetometry measurements that find that two monolayers EuO on STO are ferromagnetic, while a single monolayer remains paramagnetic [26].

Increasing the EuO thickness to 4 ML results in the same characteristics in the photoemission data as observed for 2 ML although with lower intensity due to stronger scattering of the photoelectrons from the interface in the now thicker EuO layer. Experimental evidence for a finite spin polarization of the EuO/STO interfacial 2DEG for EuO overlayer thicknesses larger than 2 ML and calculations predicting an even increased Ti magnetic moment for three instead of two monolayers of EuO strongly suggest that the threshold EuO thickness for obtaining spin polarization in the redox-created 2DEG at the EuO/STO interface is as low as 2 ML.

We assume that at finite temperature the induced Ti magnetic moment scales with the size of the Eu magnetic moment. In a very recent work we showed that a magnetic proximity effect at 3d ferromagnet/EuO interfaces enhances the magnetic order in EuO effectively in the 2D limit [31]. We therefore believe that the degree of spin polarization of the 2DEG at the EuO/STO interface can be significantly enhanced by depositing a 3d ferromagnet overlayer on top of the few monolayer thin EuO on STO.

In summary, we studied the spin polarization of the redox-created 2DEG at the EuO/STO(001) interface by circular dichroism in ToF-MM and DFT + U calculations. We found that the 2DEG is significantly spin polarized due to the proximity to the ferromagnetic EuO overlayer. The threshold EuO thickness for inducing spin polarization is as low as 2 ML. Since the magnetic order of EuO can be enhanced further by other proximity effects, the EuO/STO(001) interface turns out to serve as an ideal template for creating (multi-)functional spin-polarized 2DEGs for application in oxide electronics.

ACKNOWLEDGMENTS

This work was supported by the Deutsche Forschungsgemeinschaft through Sonderforschungsbereich SFB 1432 (Project No. 425217212, Subproject No. B03) and Transregio TRR 173 (Project No. 268565370, Subproject No. A02) and by the German Federal Ministry of Education and Research under framework program ErUM (Projects No. 05K22VL1 and No. 05K22UM1). We acknowledge DESY (Hamburg, Germany), a member of the Helmholtz Association HGF, for the provision of experimental facilities. Parts of this re-

search were carried out at PETRA III using beam line P04. Beam time was allocated for proposal I-20220420. R.P. and A.D. acknowledge support by the German Research Foundation (DFG, Deutsche Forschungsgemeinschaft) within the Collaborative Research Centre CRC 1242 (Project No. 278162697, Subproject No. C02) and computational time at Gauss Center for Supercomputing, *SuperMUC-NG* (*Leibniz Rechenzentrum*), project pr87ro.

DATA AVAILABILITY

The data supporting this study's findings are available within the article.

[1] A. Ohtomo and H. Y. Hwang, A high-mobility electron gas at the $LaAlO_3/SrTiO_3$ heterointerface, Nature (London) **427**, 423 (2004).

[2] A. Brinkman, M. Huijben, M. Van Zalk, J. Huijben, U. Zeitler, J. Maan, W. G. van der Wiel, G. Rijnders, D. H. Blank, and H. Hilgenkamp, Magnetic effects at the interface between non-magnetic oxides, Nature Mater. **6**, 493 (2007).

[3] J. A. Bert, B. Kalisky, C. Bell, M. Kim, Y. Hikita, H. Y. Hwang, and K. A. Moler, Direct imaging of the coexistence of ferromagnetism and superconductivity at the $LaAlO_3/SrTiO_3$ interface, Nature Phys. **7**, 767 (2011).

[4] W. Li, L. Gao, and A. A. Demkov, Controlling spin-polarized carriers at the $SrTiO_3$/EuO interface via the ferroelectric field effect, Phys. Rev. B **102**, 035308 (2020).

[5] J. Goniakowski, F. Finocchi, and C. Noguera, Polarity of oxide surfaces and nanostructures, Rep. Prog. Phys. **71**, 016501 (2008).

[6] H. Y. Hwang, Tuning interface states, Science **313**, 1895 (2006).

[7] A. Kalabukhov, R. Gunnarsson, J. Börjesson, E. Olsson, T. Claeson, and D. Winkler, Effect of oxygen vacancies in the $SrTiO_3$ substrate on the electrical properties of the $LaAlO_3/SrTiO_3$ interface, Phys. Rev. B **75**, 121404(R) (2007).

[8] G. Herranz, M. Basletić, M. Bibes, C. Carrétéro, E. Tafra, E. Jacquet, K. Bouzehouane, C. Deranlot, A. Hamzić, J.-M. Broto, A. Barthélémy, and A. Fert, High mobility in $LaAlO_3/SrTiO_3$ heterostructures: Origin, dimensionality, and perspectives, Phys. Rev. Lett. **98**, 216803 (2007).

[9] K. J. Kormondy, A. B. Posadas, T. Q. Ngo, S. Lu, N. Goble, J. Jordan-Sweet, X. P. A. Gao, D. J. Smith, M. R. McCartney, J. G. Ekerdt, and A. A. Demkov, Quasi-two-dimensional electron gas at the epitaxial alumina/$SrTiO_3$ interface: Control of oxygen vacancies, J. Appl. Phys. **117**, 095303 (2015).

[10] B. I. Edmondson, S. Liu, S. Lu, H. Wu, A. Posadas, D. J. Smith, X. P. A. Gao, A. A. Demkov, and J. G. Ekerdt, Effect of $SrTiO_3$ oxygen vacancies on the conductivity of $LaTiO_3/SrTiO_3$ heterostructures, J. Appl. Phys. **124**, 185303 (2018).

[11] C. Lin and A. A. Demkov, Electron correlation in oxygen vacancy in $SrTiO_3$, Phys. Rev. Lett. **111**, 217601 (2013).

[12] K. J. Kormondy, L. Gao, X. Li, S. Lu, A. B. Posadas, S. Shen, M. Tsoi, M. R. McCartney, D. J. Smith, J. Zhou, L. L. Lev, M.-A. Husanu, V. N. Strocov, and A. A. Demkov, Large positive linear magnetoresistance in the two-dimensional t_{2g} electron gas at the EuO/$SrTiO_3$ interface, Sci. Rep. **8**, 7721 (2018).

[13] M. Zapf, M. Schmitt, J. Gabel, P. Scheiderer, M. Stübinger, B. Leikert, G. Sangiovanni, L. Dudy, S. Chernov, S. Babenkov, D. Vasilyev, O. Fedchenko, K. Medjanik, Y. Matveyev, A. Gloskowski, C. Schlueter, T.-L. Lee, H.-J. Elmers, G. Schönhense, M. Sing, and R. Claessen, Hard x-ray angle-resolved photoemission from a buried high-mobility electron system, Phys. Rev. B **106**, 125137 (2022).

[14] C. Chen, L. Fang, J. Zhang, G. Zhao, and W. Ren, Thickness control of the spin-polarized two-dimensional electron gas in $LaAlO_3/BaTiO_3$ superlattices, Sci. Rep. **8**, 467 (2018).

[15] B. R. K. Nanda and S. Satpathy, Spin-polarized two-dimensional electron gas at oxide interfaces, Phys. Rev. Lett. **101**, 127201 (2008).

[16] Z. Gui and A. Janotti, Carrier-density-induced ferromagnetism in $EuTiO_3$ bulk and heterostructures, Phys. Rev. Lett. **123**, 127201 (2019).

[17] H.-S. Lu, T.-Y. Cai, S. Ju, and C.-D. Gong, Half-metallic $LaAlO_3/EuTiO_3$ heterointerface from density-functional theory, Phys. Rev. Appl. **3**, 034011 (2015).

[18] D. Stornaiuolo, C. Cantoni, G. M. De Luca, R. Di Capua, E. Di. Gennaro, G. Ghiringhelli, B. Jouault, D. Marrè, D. Massarotti, F. Miletto Granozio, I. Pallecchi, C. Piamonteze, S. Rusponi, F. Tafuri, and M. Salluzzo, Tunable spin polarization and superconductivity in engineered oxide interfaces, Nature Mater. **15**, 278 (2016).

[19] R. Di Capua, M. Verma, M. Radovic, V. N. Strocov, C. Piamonteze, E. B. Guedes, N. C. Plumb, Y. Chen, M. D'Antuono, G. M. D. Luca, E. D. Gennaro, D. Stornaiuolo, D. Preziosi, B. Jouault, F. M. Granozio, A. Sambri, R. Pentcheva, G. Ghiringhelli, and M. Salluzzo, Orbital selective switching of ferromagnetism in an oxide quasi two-dimensional electron gas, npj Quantum Mater. **7**, 41 (2022).

[20] R. Di Capua, M. Verma, M. Radović, N. C. Plumb, J. H. Dil, Z. Ristić, E. B. Guedes, G. M. De Luca, D. Preziosi, Z. Wang, A. P. Weber, R. Pentcheva, and M. Salluzzo, Two-dimensional electron gas at the (001) surface of ferromagnetic $EuTiO_3$, Phys. Rev. Res. **3**, L042038 (2021).

[21] H. Zhang, Y. Yun, X. Zhang, H. Zhang, Y. Ma, X. Yan, F. Wang, G. Li, R. Li, T. Khan, Y. Chen, W. Liu, F. Hu, B. Liu, B. Shen, W. Han, and J. Sun, High-mobility spin-polarized two-dimensional electron gases at EuO/$KTaO_3$ interfaces, Phys. Rev. Lett. **121**, 116803 (2018).

[22] L. Gao and A. A. Demkov, Spin-polarized two-dimensional t_{2g} electron gas: *Ab initio* study of EuO interface with oxygen-deficient $SrTiO_3$, Phys. Rev. B **97**, 125305 (2018).

[23] J. Lee, N. Sai, and A. A. Demkov, Spin-polarized two-dimensional electron gas through electrostatic doping in $LaAlO_3$/EuO heterostructures, Phys. Rev. B **82**, 235305 (2010).

[24] Y. Wang, M. K. Niranjan, J. D. Burton, J. M. An, K. D. Belashchenko, and E. Y. Tsymbal, Prediction of a spin-polarized two-dimensional electron gas at the $LaAlO_3$/EuO (001) interface, Phys. Rev. B **79**, 212408 (2009).

[25] P. V. Lukashev, A. L. Wysocki, J. P. Velev, M. van Schilfgaarde, S. S. Jaswal, K. D. Belashchenko, and E. Y. Tsymbal, Spin filtering with EuO: Insight from the complex band structure, Phys. Rev. B **85**, 224414 (2012).

[26] P. Lömker, T. C. Rödel, T. Gerber, F. Fortuna, E. Frantzeskakis, P. Le Fèvre, F. Bertran, M. Müller, and A. F. Santander-Syro, Two-dimensional electron system at the magnetically tunable EuO/$SrTiO_3$ interface, Phys. Rev. Mater. **1**, 062001(R) (2017).

[27] G. Schmidt, D. Ferrand, L. W. Molenkamp, A. T. Filip, and B. J. van Wees, Fundamental obstacle for electrical spin injection from a ferromagnetic metal into a diffusive semiconductor, Phys. Rev. B **62**, R4790 (2000).

[28] C. Caspers, M. Müller, A. X. Gray, A. M. Kaiser, A. Gloskovskii, C. S. Fadley, W. Drube, and C. M. Schneider, Electronic structure of EuO spin filter tunnel contacts directly on silicon, Physica Rapid Res. Ltrs. **5**, 441 (2011).

[29] C. Caspers, A. Gloskovskii, M. Gorgoi, C. Besson, M. Luysberg, K. Z. Rushchanskii, M. Ležaić, C. S. Fadley, W. Drube, and M. Müller, Interface engineering to create a strong spin filter contact to silicon, Sci. Rep. **6**, 22912 (2016).

[30] S. Datta and B. Das, Electronic analog of the electro-optic modulator, Appl. Phys. Lett. **56**, 665 (1990).

[31] P. Rosenberger, M. Kundu, A. Gloskovskii, C. Schlueter, U. Nowak, and M. Müller, Proximity coupling induced two dimensional magnetic order in EuO-based synthetic ferrimagnets, Sci. Rep. **14**, 21586 (2024).

[32] D. Mönkebüscher, P. Rosenberger, F. Mertens, R. Adam, C. M. Schneider, U. Parlak, M. Müller, and M. Cinchetti, Modulation of the transient magnetization of an EuO/Co bilayer tuned by optical excitation, Adv. Mater. Interfaces **10**, 2300236 (2023).

[33] T. S. Santos, J. S. Moodera, K. V. Raman, E. Negusse, J. Holroyd, J. Dvorak, M. Liberati, Y. U. Idzerda, and E. Arenholz, Determining exchange splitting in a magnetic semiconductor by spin-filter tunneling, Phys. Rev. Lett. **101**, 147201 (2008).

[34] M. Müller, G.-X. Miao, and J. S. Moodera, Exchange splitting and bias-dependent transport in EuO spin filter tunnel barriers, Europhys. Lett. **88**, 47006 (2009).

[35] G.-X. Miao, M. Müller, and J. S. Moodera, Magnetoresistance in double spin filter tunnel junctions with nonmagnetic electrodes and its unconventional bias dependence, Phys. Rev. Lett. **102**, 076601 (2009).

[36] T. Heider, T. Gerber, O. Köksal, M. Eschbach, E. Młyńczak, P. Lömker, P. Gospodaric, M. Gehlmann, M. Plötzing, R. Pentcheva, L. Plucinski, C. M. Schneider, and M. Müller, Temperature-dependent spin-resolved electronic structure of EuO thin films, Phys. Rev. B **106**, 054424 (2022).

[37] N. Jutong, I. Rungger, C. Schuster, U. Eckern, S. Sanvito, and U. Schwingenschlögl, Electronic transport through EuO spin-filter tunnel junctions, Phys. Rev. B **86**, 205310 (2012).

[38] J. Viefhaus, F. Scholz, S. Deinert, L. Glaser, M. Ilchen, J. Seltmann, P. Walter, and F. Siewert, The variable polarization XUV Beamline P04 at PETRA III: Optics, mechanics and their performance, Nucl. Instrum. Meth. Phys. Res. A **710**, 151 (2013), The 4th international workshop on Metrology for X-ray Optics, Mirror Design, and Fabrication.

[39] K. Medjanik, O. Fedchenko, S. Chernov, D. Kutnyakhov, M. Ellguth, A. Oelsner, B. Schönhense, T. R. F. Peixoto, P. Lutz, C.-H. Min, F. Reinert, S. Däster, Y. Acremann, J. Viefhaus, W. Wurth, H. J. Elmers, and G. Schönhense, Direct 3D mapping of the Fermi surface and Fermi velocity, Nature Mater. **16**, 615 (2017).

[40] O. Fedchenko, J. Minár, A. Akashdeep, S. W. D'Souza, D. Vasilyev, O. Tkach, L. Odenbreit, Q. Nguyen, D. Kutnyakhov, N. Wind, L. Wenthaus, M. Scholz, K. Rossnagel, M. Hoesch, M. Aeschlimann, B. Stadtmüller, M. Kläui, G. Schönhense, T. Jungwirth, A. B. Hellenes, G. Jakob, L. Šmejkal, J. Sinova, and H.-J. Elmers, Observation of time-reversal symmetry breaking in the band structure of altermagnetic RuO_2, Sci. Adv. **10**, eadj4883 (2024).

[41] O. Tkach, S. Fragkos, Q. Nguyen, S. Chernov, M. Scholz, N. Wind, S. Babenkov, O. Fedchenko, Y. Lytvynenko, D. Zimmer, A. Hloskovskii, D. Kutnyakhov, F. Pressacco, J. Dilling, L. Bruckmeier, M. Heber, F. Scholz, J. Sobota, J. Koralek, N. Sirica *et al.*, Multi-mode front lens for momentum microscopy: Part II experiments, arXiv:2401.10084.

[42] P. Rosenberger and M. Müller, Europium oxide: Growth guide for the first monolayers on oxidic substrates, Phys. Rev. Mater. **6**, 044404 (2022).

[43] P. Lömker and M. Müller, Redox-controlled epitaxy and magnetism of oxide heterointerfaces: EuO/$SrTiO_3$, Phys. Rev. Mater. **3**, 061401(R) (2019).

[44] M. Müller, P. Lömker, P. Rosenberger, M. Hussein Hamed, D. N. Mueller, R. A. Heinen, T. Szyjka, and L. Baumgarten, Hard X-ray photoelectron spectroscopy of tunable oxide interfaces, J. Vac. Sci. Technol. A **40**, 013215 (2022).

[45] P. Rosenberger, Emerging phenomena at EuO ultrathin film interfaces in the spotlight of photoelectron spectroscopy, Ph.D. thesis, Universität Konstanz, 2024, http://nbn-resolving.de/urn:nbn:de:bsz:352-2-1ikj3r3orzr7h8.

[46] G. Berner, M. Sing, H. Fujiwara, A. Yasui, Y. Saitoh, A. Yamasaki, Y. Nishitani, A. Sekiyama, N. Pavlenko, T. Kopp, C. Richter, J. Mannhart, S. Suga, and R. Claessen, Direct k-space mapping of the electronic structure in an oxide-oxide interface, Phys. Rev. Lett. **110**, 247601 (2013).

[47] C. Westphal, J. Bansmann, M. Getzlaff, and G. Schönhense, Circular dichroism in the angular distribution of photoelectrons from oriented CO molecules, Phys. Rev. Lett. **63**, 151 (1989).

[48] C. M. Schneider, M. S. Hammond, P. Schuster, A. Cebollada, R. Miranda, and J. Kirschner, Observation of magnetic circular dichroism in uv photoemission from ferromagnetic fcc cobalt films, Phys. Rev. B **44**, 12066 (1991).

[49] W. Kuch and C. M. Schneider, Magnetic dichroism in valence band photoemission, Rep. Prog. Phys. **64**, 147 (2001).

[50] G. Kresse and J. Hafner, *Ab initio* molecular dynamics for liquid metals, Phys. Rev. B **47**, 558 (1993).

[51] G. Kresse and J. Furthmüller, Efficiency of *ab-initio* total energy calculations for metals and semiconductors using a plane-wave basis set, Comput. Mater. Sci. **6**, 15 (1996).

[52] P. E. Blöchl, Projector augmented-wave method, Phys. Rev. B **50**, 17953 (1994).

[53] G. Kresse and D. Joubert, From ultrasoft pseudopotentials to the projector augmented-wave method, Phys. Rev. B **59**, 1758 (1999).

[54] J. P. Perdew, A. Ruzsinszky, G. I. Csonka, O. A. Vydrov, G. E. Scuseria, L. A. Constantin, X. Zhou, and K. Burke, Restoring the density-gradient expansion for exchange in solids and surfaces, Phys. Rev. Lett. **100**, 136406 (2008).

[55] S. L. Dudarev, G. A. Botton, S. Y. Savrasov, C. J. Humphreys, and A. P. Sutton, Electron-energy-loss spectra and the structural stability of nickel oxide: An LSDA+U study, Phys. Rev. B **57**, 1505 (1998).

[56] H. O. Jeschke, J. Shen, and R. Valentí, Localized versus itinerant states created by multiple oxygen vacancies in $SrTiO_3$, New J. Phys. **17**, 023034 (2015).